WCTE 2018
2018 World Conference on Timber Engineering
August 20 - 23, 2018 | Seoul, Republic of Korea

A STOCHASTIC FINITE ELEMENT MODEL FOR GLULAM BEAMS OF HARDWOODS

Cristóbal Tapia Camú[1], **Simon Aicher**[2]

ABSTRACT: A stochastic finite element model for the prediction of the bending strength of glulam beams made of oak is presented. The model uses a statistical approach for the generation of the mechanical properties, considering experimental statistical distributions and correlations between several variables. Special emphasis is laid on the simulation of the variation of the mechanical properties along each single board, for which an autoregressive model is used, which also considers the cross-correlation between elastic modulus and tensile strength. The extended finite element method is used for the modelling of crack initiation and evolution, where tensile strengths and failure energies are taken into account. The model is calibrated with a series of experimental tests, performed at the MPA, University of Stuttgart, with glulam beams made of oak. The results of the simulations are presented and discussed.

KEYWORDS: strength model, glulam, hardwood, XFEM

1 INTRODUCTION

The use of hardwood species in timber structures has been on the rise for the last years, especially in Europe, which is expressed in a growing use of oak and beech for building purposes. The reasons for this development are multiple, and can be found, among others, in an under-use of over-aging hardwood forests, architectural aspects and, most important, in the observed higher values for strength and stiffness when compared to softwood values. Nevertheless, it is only in the form of processed engineered timber products, such as glued laminated timber (GLT), laminated veneer lumber (LVL) and cross-laminated timber (CLT), where these benefits can be fully taken advantage of. However, before a broader use of the hardwood material can be made, specific challenges have to be addressed.

For the case of glulam, today a European standardization framework for the production and product characteristics of GLT made of hardwood species, similar to EN 14080 [1] (the European softwood GLT standard), is lacking. The existing CE-marked hardwood GLT products made of oak, beech and chestnut are based on a CUAP (Common Understanding Approval Procedure), prescribing a fully experimentally-based route to the certification. This is obviously very cost intensive. A new EAD (European Approval Document) based on test-assisted calculations would definitively help to lower the production costs by requiring a smaller amount of tests to be performed. Unfortunately, given the relatively lower strength observed for finger-joints in hardwood species, especially of higher densities —producing a different characteristic distribution of weak spots in the beam— the use of the current models for softwood glulam are deemed to be inadequate to correctly represent the mechanical behavior of hardwood glulams.

In the context of the EU-Hardwoods Project [2], a new finite element model was developed, capable of predicting the characteristic bending strength of hardwood glulam beams. This is achieved by means of the application of the Monte-Carlo method, where the variables correspond to the different mechanical properties of the constituent boards. Different to previous pioneering FEM models by Ehlbeck *et al.* [3], Blaß *et al.* [4] and Frese *et al.* [5], the new model considers more advanced modeling techniques and failure criteria. These include the use of the extended finite element method (XFEM) in conjunction with traction separation laws based on energies, as well as a wider range of stochastic variables, which are taken into account to obtain better correlations between the simulations and experimental results.

2 GENERAL ASPECTS OF A STRENGTH MODEL

The use of stochastic FE models for the prediction of bending strength in glulam has been an important research field since the mid 80's, being fundamental for the development of the current design provisions contained in the European standard EN 14080 [1]. These models, starting with the work of Ehlbeck *et al.* [3], moving forward to the more recent implementations of Blaß *et al.* [4] or Fink [6], are all based on the same principles. At its core, the GLT model reduces to the statistical reproduction of the mechanical behavior of the laminations, i.e. of the boards, and the finger-joints connecting the boards lengthwise.

[1] Cristóbal Tapia, MPA, University of Stuttgart, Germany, cristobal.tapia-camu@mpa.uni-stuttgart.de
[2] Simon Aicher, MPA, University of Stuttgart, Germany, simon.aicher@mpa.uni-stuttgart.de

Implemented in a correct manner, the model yields the observed global behavior of the glulam beams. For this purpose, the modulus of elasticity (MOE) and strength values are set to vary locally along the length of each board, which are further differentiated by different global, i.e. integral properties at the board level. This allows for the reproduction of the observed distribution of weak spots —normally, but not exclusively represented by knots. The exact manner in which this properties are assigned to each region (or *cells*) may vary from model to model, but in all implementations an intrinsic stochastic component is present, which is based on experimental tests and allows for the utilization of the Monte-Carlo method. This model, combined with appropriate failure criteria, sets the basis for what in this context is known as a strength model.

This approach allows for the possibility to better correlate the properties of individual boards and their respective finger-joints to the ones of the glulam beams that are built from them, hereby reducing the amount of expensive tests needed for a safe assertion of the characteristic beam values. However, before such a model can be used to this end in the real world, it needs to be calibrated with different datasets, which will provide an adequate degree of confidence in the model. The following sections describe, in a compact manner, the methodology used to build a stochastic finite element model that implements the above described concepts, where a specific dataset of oak is used.

3 GENERATION OF THE MATERIAL PROPERTIES

The generation of the material properties is a key aspect of the model. As such, the applied methodology needs to be able to reproduce the observed mechanical characteristics, i.e. the relevant aspects of the boards and finger-joints that determine the global behavior of the glulam, in a reliable manner. The implemented method considers a three step process. First, a set of global properties for each board is generated, which include MOE, tensile and compressive strength, and the length of each board. In the next step, an autoregressive process is used to generate the varying mechanical properties along the boards, for which the previously generated global properties are used. A simple, light-modified vector-autoregressive model is used to account for the cross-correlation between modulus of elasticity and strength values. The final step considers the generation of the properties for the finger-joints, using, to this end, the mechanical properties generated in the second step.

3.1 BOARD PROPERTIES AT GLOBAL LEVEL

The process to simulate the required material properties for the model starts with the generation of a set of global mechanical properties for each lamination of the glulam build-up. This means, that values for MOE, tensile strength ($f_{t,0}$) and compressive strength ($f_{0,c}$) are generated, starting from the respective known statistical distributions. These values are at the same time correlated between each other by means of the coefficients given in Table 1. In order to reproduce these correlations, a common procedure described in [7] is applied. The method can be summarized by the following steps:

1. Samples of a normal distribution $\mathcal{N}(0,1)$ are independently generated for each of the random variables (MOE, $f_{t,0}$ and $f_{c,0}$) and stored in separate columns in a matrix $\boldsymbol{R}$.

2. Given the correlation matrix $\boldsymbol{C}$, a matrix $\boldsymbol{U}$ is derived, satisfying the condition

$$\boldsymbol{U}^T\boldsymbol{U} = \boldsymbol{C}. \tag{1}$$

   Eq. (1) is solved by means of a square root decomposition. Other decompositions are also possible, but may give slightly different results.

3. The set of correlated data $\boldsymbol{R_c}$ is computed according to

$$\boldsymbol{R_c} = \boldsymbol{R}\boldsymbol{U}, \tag{2}$$

   which correspond to correlated variables of the (auxiliary) $\mathcal{N}(0,1)$ distributions.

4. These results need to be mapped into the distributions corresponding to each mechanical property. For this, the *cumulative distribution function* of these variables (in $\mathcal{N}(0,1)$) is computed. These values are then fed to the *percent point function* of the corresponding distributions, which delivers the needed correlated data.

Applying the described algorithm to the experimental correlations and distributions defined in Table 1 and 2, a dataset for the global mechanical properties of the boards was generated. Figure 1a shows the obtained MOE-$f_{t,0}$-correlation. It can be observed, that each of the variable samples (MOE and $f_{t,0}$) follows their corresponding distribution (see Figures 1b,c), while maintaining a correlation $R = 0.48$ (see Figure 1a), which is exactly the value given as input (see Table 1).

The length for each board is generated during this step too. This is simply done by directly generating a sample from the corresponding statistical distribution, which in this case is assumed to be a *lognormal* distribution.

3.2 VARIATION OF PROPERTIES ALONG EACH BOARD

An important point consists on the correct implementation of the variation of the different mechanical properties

Table 1: *Coefficients of correlation used for the generation of the global mechanical properties. First three rows and columns ($f_{t,0}$, $f_{c,0}$ and E_0) correspond to the matrix* $\boldsymbol{C}$

	$f_{t,0}$	$f_{c,0}$	E_0	$f_{t,\mathrm{fj}}$
$f_{t,0}$	1	0.8*	0.48	—
$f_{c,0}$	0.8*	1	0.8	—
E_0	0.48	0.8	1	0.15
$f_{t,\mathrm{fj}}$	—	—	0.15	1

* Assumed values, since no data is available.

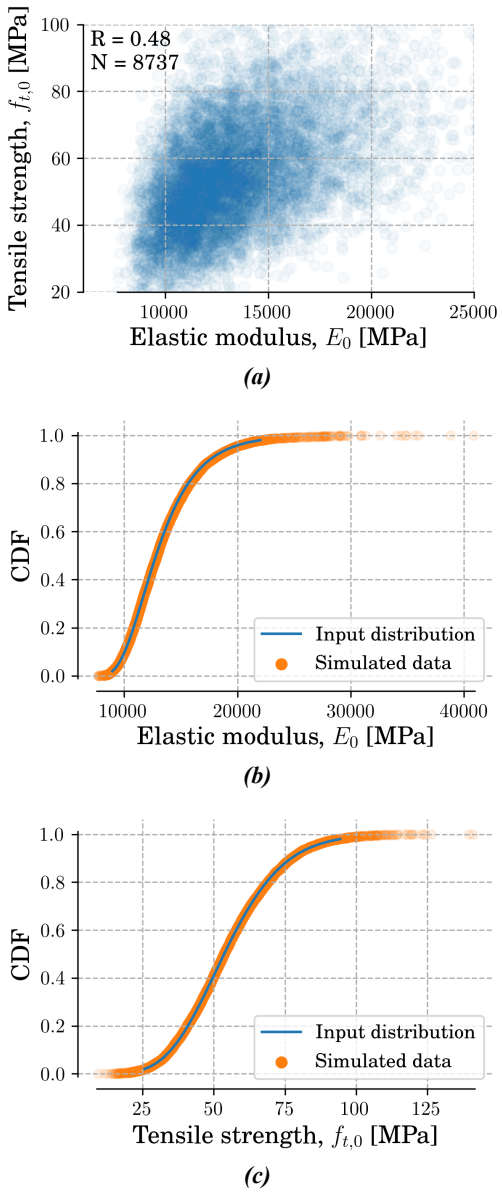

Figure 1: *(a) Example of generated correlated data for MOE and $f_{t,0}$; (b) and (c) cumulative distribution function of the generated data and the input distribution for the MOE (E_0) and tensile strength ($f_{t,0}$), respectively.*

along each single board, since this has a dominant impact on the so-called *lamination effect*. For this, the approach used by Kline *et al.* [8] and Taylor *et al.* [9] was implemented, which represents the variation of the MOE and strength along each board as an autoregressive model. In its general form, an autoregressive model for a variable X_t (MOE or MOR) of order p has the form

$$X_t = C + \sum_{i=1}^{p} \varphi_i X_{t-i} + \varepsilon_t, \tag{3}$$

where the values φ_i are the parameters of the model, C is a constant and ε_t is white noise. The data generated by this process will normally deviate from the global value assigned to the board—in the sense that e.g. the MOE computed from the single cells will not match the MOE given to the whole board—, which is a result of the stochastic

Table 2: *Statistical distributions used for the generation of the mechanical properties and the length of the boards, ℓ. All variables are assumed to follow a lognormal distribution with fitted parameters* shape, loc *and* scale. *The data corresponds to LS13 boards.*

Params.	shape	loc	scale
E_0 :	0.4261	6224.78	6583.90
$f_{t,0}$:	0.1838	−35.23	88.86
$f_{c,0}$:	0.0461	−0.2263	50.25
$f_{t,\mathrm{fj}}$:	0.5569	24.69	15.23
ℓ :	0.8695	484.70	125.23

nature of the method. A correction is, therefore, required. For the case of the MOE, this is done by shifting the data so that the equivalent stiffness of the board, computed from the individual values of each cell, matches the global stiffness. The equivalent MOE is computed by means of the equation for serial springs (k_i, K_{eq} = cell and total board stiffness)

$$\frac{L}{AE_{\mathrm{eq}}} = \frac{1}{K_{\mathrm{eq}}} = \sum_i \frac{1}{k_i} = \sum_i \frac{\ell_i}{AE_i}, \tag{4}$$

and the difference between this value and the assigned global MOE is calculated. This difference is then added (summed) to the generated data. In order to obtain a small error between this two values, this process has to be repeated in an iterative way. In this case, five iterations were used, which results in a negligible error.

For the generation of the strength data along the board, the concept of the vector autoregressive model (VAR) was applied, which is used to correlate different time-series-like variables. However, differently as in a typical VAR model, the generated data are based on the already generated (autocorrelated) X_t data for the MOE. For this, the lag-0 cross-correlation between the MOE and $f_{t/c,0}$ is used. The model takes the following form:

$$Y_t = C + \psi_0 X_t + \varepsilon_t, \tag{5}$$

where Y are the data needed to be generated (strength), X are the data to be correlated to (MOE) and ψ_0 is the model parameter corresponding to the lag-0 cross-correlation. C and ε_t have the same meaning as before. Similar as for the MOE-data, a correction is applied to the strength values, which consists on shifting the data so that the minimum value of each board equals the assigned strength of the board. It is important to mention, that the variables X and Y of Eqs. (3) and (5) are generated initially with $\mathcal{N}(0,1)$ distributions for the white noise, and then, similar to the previous step, *mapped* to the needed distributions. These are normal distributions with $\mu = E_{0,\mathrm{board}}$ and a standard deviation according to the coefficients of variation (COV) shown in Table 3. This helps in the determination of the model parameter ψ_0 of Eq. (5) since otherwise variables of different orders of magnitude would be mixed (MOE and $f_{t,0}$).

The length of each cell chosen for the simulations was 100 mm, which, in contrast to the windows of approx.

Table 3: *Coefficients of variations (COV) for the MOE and tensile strength used for the generation of properties within each board, for different board strength classes*

Board class	MOE	$f_{t,0}$
LS13	5 %	10 %
LS10	15 %	15 %

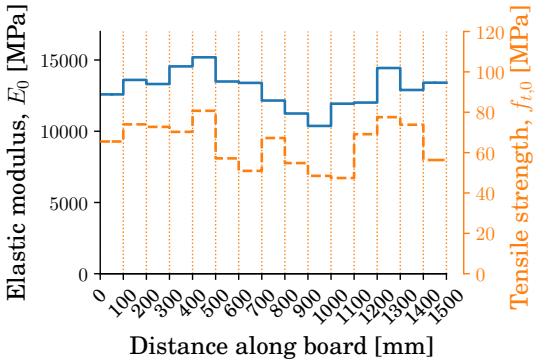

(a)

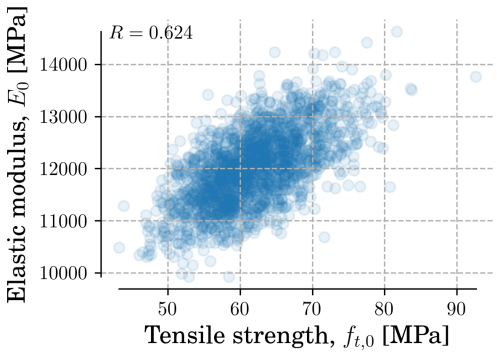

(b)

Figure 2: *Generation of correlated and cross-correlated mechanical properties within a single board. (a) MOE and tensile strength (dashed line) generated for a 1500 mm long board; (b) cross-correlation between MOE and $f_{t,0}$ for a fictive, very long board (ℓ = 200 m), containing 2000* cells.

600 mm used in [9], offer a higher resolution for the variation of the material properties. Recent, not-yet published experimental results seem to indicate that a first order AR model should give good results for the shorter cells of 100 mm. Here, the lag-1 correlation coefficient is taken as $r_1 = 0.6$, which has been obtained from the mentioned experimental results. For an AR(1) model, $r_1 = \varphi_1$, so that the value can be directly used in the Eq. (3). It is currently not possible (or very difficult) to gather the necessary experimental data, that would allow the computation of the lag-0 cross-correlation of the variable pairs MOE-$f_{t,0}$ along the board. Nevertheless, the lag-0 cross-correlation value for MOE-$f_{t,0}$ has been obtained at the positions corresponding to $\min\{f_{t,0}\}$ (i.e. at the failure position). Experimental results gave a value for this cross-correlation of 0.65; this value will be assumed as the lag-0 cross-correlation for each cell of the board: $\psi_0 = 0.65$.

Figure 2a shows one example of the generated data, where both the MOE and strength variation along the board can be seen. The length of the board was chosen as ℓ = 1500 mm, so that the cross-correlated variation can be better appreciated; the length of the boards used in the following simulations is approximately 600 mm. It can be observed how both variables follow very roughly the same pattern, which is explained by the used cross-correlation coefficient of 0.65.

In order to check weather the used cross-correlation is having the desired effect in the generation of the properties within the board, a single, fictive, very long board is created (ℓ = 200 m). Given the typical length of a generated board (600 mm to 3000 mm), the number of cells produced (6 to 30) would not be enough to show the true nature of the simulated stochastic process. Figure 2b shows the mentioned lag-0 cross-correlation obtained for the long board, where a value $R = 0.624$ can be observed, which is close to the input value of 0.65.

3.3 ASSIGNMENT OF TENSILE STRENGTHS FOR THE FINGER-JOINTS

The procedure to generate the mechanical properties for the finger-joints applies, in essence, the same method as for the generation of the properties of the individual boards. However, a further step is introduced, as the data generated for the finger joints are correlated to the mean value of the MOEs corresponding to the jointed cells ($E_{\text{ij,mean}} = 0.5(E_i + E_j)$). For this, it is a prerequisite that the data corresponding to the boards have been generated in a previous step, which means that a certain *order* needs to be respected. By *order* it is meant that the vector containing the values for the MOEs has been defined, and thus, also the values for $E_{\text{ij,mean}}$, denoted here as $\boldsymbol{E}_{\text{fj}}$. The problem is then to generate the correlated data for the tensile strength of the finger-joints, $f_{t,\text{fj}}$, and $E_{\text{ij,mean}}$, where one of the vectors ($\boldsymbol{E}_{\text{fj}}$) is given. This differs from the method explained in Section 3.1, where all data vectors were simultaneously generated.

If $\boldsymbol{E}$ and $\boldsymbol{T}$ are the vectors for MOE and $f_{t,\text{fj}}$, respectively, which were randomly generated with the procedure described in Section 3.1, then the extra steps necessary to order them are:

1. obtain the indices that sort $\boldsymbol{E}_{\text{fj}}$ and store them in the variable $\boldsymbol{I}_j$,
2. get the indices that sort $\boldsymbol{E}$ and store them as $\boldsymbol{I}_k$,
3. sort the vector $\boldsymbol{T}$ according to the indices $\boldsymbol{I}_k$, which will give a vector $\boldsymbol{T}^*$,
4. and finally sort the vector $\boldsymbol{T}^*$ with the indices $\boldsymbol{I}_j$, which will return the desired vector $\boldsymbol{f}_{\text{t,fj}}$.

The results obtained from this method will only be accurate if the size of the sample is large enough ($N \gtrapprox 500$), which is guaranteed for these simulations, since the number of boards generated are in the order of thousands. An example of the generated data is shown in Figure 3, where a total of N = 8736 finger-joints were generated and successfully correlated to the given vector $\boldsymbol{E}_{\text{fj}}$, as can be seen from the correlation coefficient $R = 0.12$. (Note: The input value was 0.15 (see Table 1), which actually corresponds to the correlation between the mean of the global dynamic MOEs of both jointed boards and $f_{t,\text{fj}}$.)

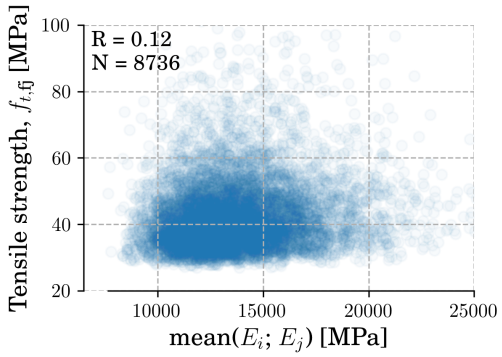

(a)

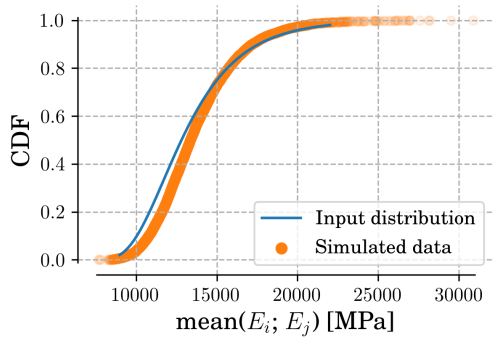

(b)

Figure 3: *Example of generated data for the finger-joints. (a) shows the obtained correlation (or lack of it) between the tensile strength of the finger-joint and the mean value of the MOEs of the cells on each side; (b) shows the cumulative distribution function for the generated MOE data and the input distribution, used to generate the global values.*

4 FINITE ELEMENT MODEL

4.1 GENERAL

The developed finite element model reproduces the bending test conditions according to EN 408 [10]. The mechanical properties of the beam are considered to vary throughout the geometry, following a layered pattern that represents the different laminations which compose the GLT. For this, the methods described in Section 3 were applied. In general, the model implements many of the concepts introduced in previous similar models [3, 4, 6], but at the same time incorporates new relevant parameters and modelling techniques, such as the extended finite element method (XFEM). One of the main characteristics of the model consists in the simulation of the failure by means of a non-linear fracture mechanics (NLFM) approach, for which —aware of the computational constraints this may impose— a two-dimensional model was deemed appropriate.

For the implementation of the model, the software Abaqus V2017 [11] with its standard solver was chosen. Two-dimensional, linear plain stress elements with reduced integration (CPS4R) were used to model the beam, whilst rigid line elements (R2D2) were applied in the support and loading zones. The global mechanical properties used for the model are those specified in Table 2. Those properties not given in Table 2, such as MOE perpendicular to the fiber (E_{90}) and shear modulus (G_{xy}), were chosen

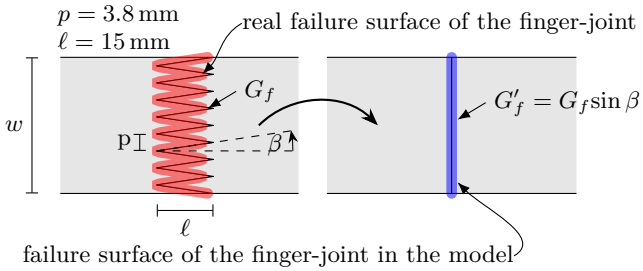

Figure 4: *Real failure surface of a finger-joint, assuming it fails along the bond line (left), and failure area in the model (right). The fracture energy G_f has to be modified accordingly, so that the total energy released in the real finger-joint and in the model are equal.*

according to EN 338 [12] and modified at each cell dependent on the value of E_0 assigned to the cell —larger values for the stiffness parallel to grain determine larger values of E_{90} and G_{xy} and vice versa.

4.2 FRACTURE ENERGIES AND FAILURE CRITERIA

The model considers crack initiation and propagation by means of NLFM, for which fracture energies and failure criteria have to be defined. Since two different materials are assumed to fail concurrently (boards=timber; finger-joints=bond line), and considering the phenomenological differences in the failure processes between them, different fracture energies were assigned to each one of them. For finger-joints, a mixed-mode $G_{f,\mathrm{fj}}$ value of 5 N/mm (5×10^3 J/m^2) was initially assumed. This value was derived from data by Serrano [13] and Stapf [14], and then normalized by the true length of the finger-joint surface, as shown in Figure 4. This energy value lead to rather low values for the bending strengths in preliminary simulations. Finally, not discussed here in detail, a higher value of 25 N/mm was used.

For the boards, a fracture energy of 10 N/mm (1×10^4 J/m^2) was assigned, which is a value that delivered satisfactory results in the model. Blank *et al.* [15] used a unique fracture energy G_f = 10 N/mm for both wood and finger-joints. The applied values lay in a physically sensible range, but are undoubtedly inversely calibrated, and will be further investigated. The failure criterion chosen corresponds to the *maximum stress criterion*, where damage initiation is related to the tensile strength of either the finger-joint or the board.

4.3 HIERARCHICAL LEVELS AND ASSIGNMENT OF MATERIAL PROPERTIES

The beam is represented through various hierarchical levels, which define the properties of the beam as a whole. Starting from the highest level, the model first defines the entire inhomogeneous beam, subdivided into three parts, representing the outer zones ($2 \times 1/6$) and the inner one (2/3). This can be visualized in the different colors of Figure 5. At this level, the different statistical parameters corresponding to the timber strength class LS10 (inner zone) and LS13 (outer zones) are assigned to each part, respectively. The next level corresponds to the sets of boards

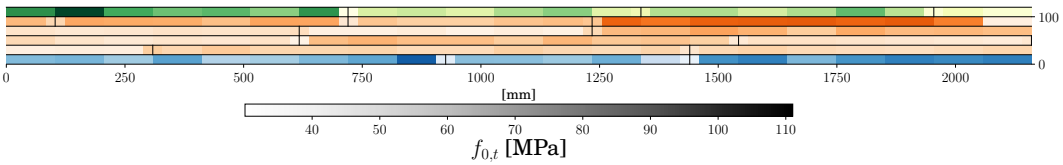

Figure 5: *Distribution of tensile strengths of the boards $f_{t,0}$ and finger-joints $F_{t,fj}$ along the whole model for a 6-lamination (1+4+1) beam. Three different colors can be appreciated: blue and green (outer regions) represent the LS13 boards; orange (middle) stands for the LS10 laminations. Finger-joints are denoted by the black vertical lines at each level. Ligher colors represent lower strengths and darker colors, higher strengths.*

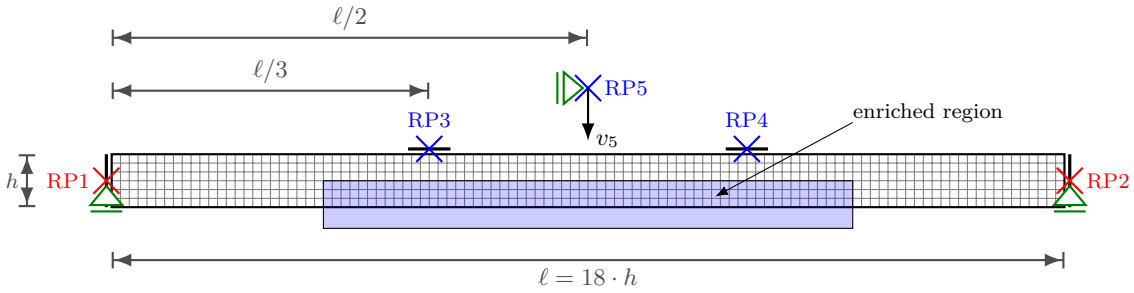

Figure 6: *Sketch of the developed finite element model, depicting the geometry, application of boundary conditions and deficition of the enriched zone needed for the XFEM method.*

that compose each one of these three parts. The boards are connected at their ends by finger-joints, which are represented in the model with a width of one element (1/3 of the thickness of the board of 20 mm), with their respective material properties (see Figure 7. Finally, each board is subdivided into *cells* with lengths of 100 mm to represent the variation of the mechanical properties within the board. The corresponding properties are assigned to each one of these cells and are later meshed with rectangular elements (aspect ratio 1:1) width edge lengths of 1/3 of the thickness of the lamination, i.e. ≈ 7 mm.

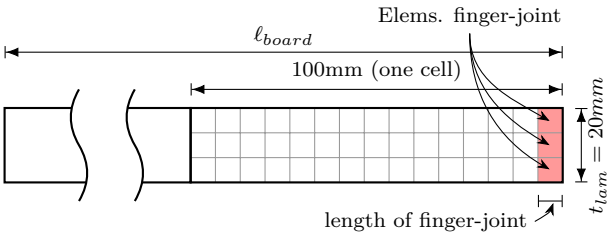

Figure 7: *Detail of the discretization of the board and definition of elements with material properties corresponding to the finger-joints*

4.4 BOUNDARY CONDITIONS

Since the model considers damage evolution for the prediction of the ultimate load, appropriate boundary conditions must be provided to guarantee the stability of the system during the solving process. The first of them concerns the loading of the beam. Since a direct application of the load at points RP3 and RP4 (see Figure 6) would lead to an unstable evolution of the system, a displacement-controlled application of the load is necessary. However, due to the random distribution of MOEs in the glulam beam, the application of vertical displacements at the reference loading points RP3 and RP4 would lead to an unequal distribution of the forces at both points. A common solution [5, 16] to overcome this effect is to model a truss-like structure, which connects both points to a third one (here RP5), which is then loaded displacement-controlled in vertical direction. This approach was further simplified in the model by the introduction of a linear equation that relates the vertical displacements v_i ($i = 3, 4, 5$) of the reference points RP3, RP4 and RP5 by

$$v_5 - 0.5 \cdot (v_3 + v_4) = 0, \tag{6}$$

ensuring that the reaction, i.e. the applied loads forces at both loading points remain equal throughout the simulation.

The second condition couples the support locations RP1 and RP2 (Figure 6) in the horizontal direction, in order to prevent uncontrolled horizontal displacements in the failing state. This is achieved by forcing the horizontal displacements u_1 and u_2 to always be of the same magnitude but move in the opposite direction:

$$u_1 + u_2 = 0. \tag{7}$$

The reference points RP1 and RP2 are attached to one-dimensional rigid elements (R2D2), arranged vertically with a length equal to the depth of the beam. These are connected to the vertical edges of the beam by means of *tie constraints*. Similarly, rigid line elements are placed horizontally at the reference points RP3 and RP4 with a load/displacements application length of 1/3 of the beam depth.

In order to capture the failure evolution of the beam, the extended finite element method was employed, for which a special region, called *enriched zone* has to be defined. This enriched regions were defined for each *cell* located

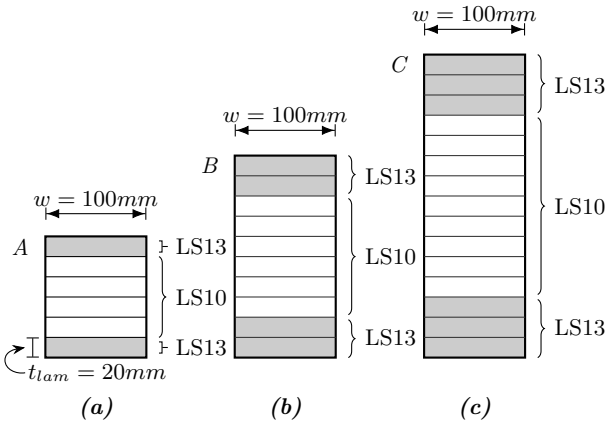

Figure 8: *Simulated composite glulam build-ups, corresponding to the experimental tests. (a) Configuration* A*: 1 LS13 + 4 LS10 + 1 LS13; (b) Configuration* B*: 2+6+2; (c) Configuration* C*: 3+9+3. The three configurations present laminations of the strength class LS13 on the outer regions and LS10 in the inner part.*

in the bending-tension area of the constant moment zone, enlarged at both ends by 1/9 of the beam's length, to account for a possible failure outside the constant moment region (see Figure 6).

5 SIMULATION RESULTS

Three series of simulations were performed for inhomogeneous beams with cross-sections of $100 \times 120\,\text{mm}^2$ (6 lams.), $100 \times 200\,\text{mm}^2$ (10 lams.) and $100 \times 300\,\text{mm}^2$ (15 lams). The three configurations are build-up with their outer laminations comprising boards of the strength class LS13, whilst the inner part is produced with laminations corresponding to the strength class LS10. Figures 8a,b,c present the composite cross-sections of the three different configurations, which from now on will be referred to as configurations *A*, *B* and *C*, respectively. A total of 672 simulations were performed for configuration *A*, 300 for configuration *B* and 250 for configuration *A*. In order to compute the bending strength of each simulated glulam beam, the first load drop-off of the *force-displacement* curve larger than 2 % was taken. A typical force-displacement curve can be seen in Figure 9, where the assumed failure criterion is marked with an arrow.

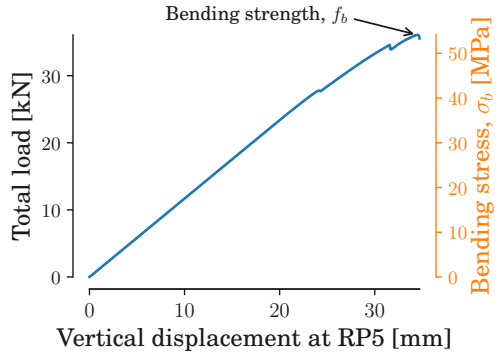

Figure 9: *Load-displacement curve for one of the simulations for configuration* B *(10 lams.). The right vertical axis shows the corresponding maximum/or nominal maximum bending stresses, σ_b. The arrow shows the point defined to be the failure point of the simulated specimen.*

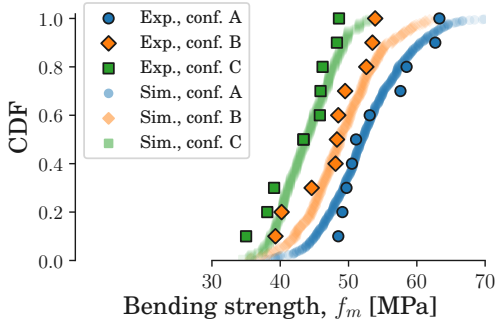

Figure 10: *Cumulative distribution functions for the experimental and simulation results, for both analyzed configurations* A*,* B *and* C*. The 300 simulations for each configurations are shown.*

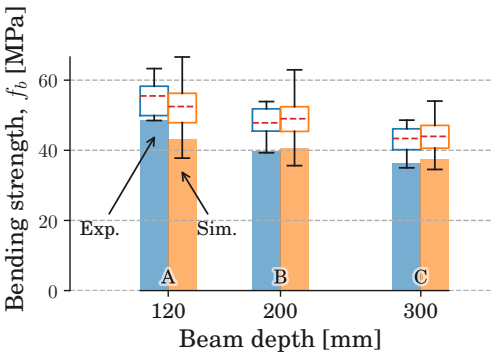

Figure 11: *Boxplots with the statistical information of the simulations and experimental data. The dashed line within each boxplot marks the mean value. The bars below them represent the 5th. percentiles, assuming a lognormal distribution of the data.*

Figures 10 and 11 show a comparison of the simulations with the respective experimental results. In general terms, the simulations capture the expected size effect, meaning that the computed bending strengths of smaller cross-sections achieve statistically higher values than larger cross-sections. This is especially well represented by the mean values (see dashed lines of the boxplots in Figure 11). The 5 % quantiles, represented by the bars of Figure 11, do express this effect, too, but its magnitude is lower than the one observed in the experimental data.

Configurations *B* and *C* present a good agreement with the experimental results at the 5th percentile level; the differences are just 1.5 % and 2.2 %. For the configuration *A*, this difference rises to 11.5 %. Table 4 presents the results for the mean and 5-percentile values for both simulation and experimental data.

The discrepancy between the simulated and experimental results of configuration *A* might have multiple causes. One explanation might be that the mesh-size for the board elements is not fine enough (currently 1/3 of the board thickness), and that configuration *A*, having a smaller cross-section, is more sensitive to this effect. The reason

for this is that the vertical (depth direction) distribution of the bending stresses, σ_b, varies within a single lamination layer fo the smaller cross-section more, as compared to larger cross-sections. A finer mesh would allow for the bending-stress variation to be better represented, which should have an impact in the crack initiation and evolution. Such an analysis would require a parametrical study, which is outside of the scope of this paper.

Table 4: *Mean and 5 %-quantile values for the simulation and experimental results. (5 % quantiles are computed assuming a lognormal distribution.)*

		Config. *A* [N/mm^2]	Config. *B* [N/mm^2]	Config. *C* [N/mm^2]
mean	Exp.	55.5	47.8	43.4
	Sim.	52.5	49.0	43.9
5 %-quant.	Exp.	48.7	39.8	36.3
	Sim.	43.2	40.5	37.5

6 CONCLUSIONS

The current state of a newly developed stochastic finite element model for the prediction of bending strength in glulam beams made of oak was presented. Regarding the methodology used and the results obtained for the analyzed data set, the following remarks can be made:

- the methodology used to generate the input material data is able to correctly represent the observed (measured) statistical distributions and correlations between the different mechanical properties at a global level.

- The use of an autoregressive model of order 1 to reproduce the variation of the mechanical properties along the board length allows both, to maintain a given coefficient of variation within the board and, at the same time, achieve a *smooth* variation of the mechanical properties. Similarly, the consideration of the cross-correlation between different variables within each board, helps to represent the laminations in a more accurate manner.

- The use of the extended finite element method, XFEM, allows for an easy manner to consider different fracture locations (initially unknown), as well as for different failure criteria, expressed by different fracture energies and strengths. This is particularly useful to clearly separate the criteria used for boards and finger-joints.

- The comparison of the simulations of glulam beams of different cross-sectional depths with experimental results showed, that the model can reproduce the empirical size effect on the mean level. On the 5th percentile level the size effect was observed, too, but its magnitude was lower than obtained with the experimental results.

- A parametrical analysis needs to be done, in order to asses the impact of different mesh-refinement levels in the simulation results, especially for the smaller cross-sections.

REFERENCES

[1] EN 14080, *Timber structures – glued laminated timber and glued solid timber – requirements*, Brussels, Belgium: European Committee for Standardization, 2013.

[2] S. Aicher, G. Dill-Langer, C. Tapia, Z. Christian, and M. Hirsch, "ERA-WoodWisdom: European hardwoods for the building sector – project part 1 (in german)," University of Stuttgart, Otto Graf Institut – Materials Testing Institute, Stuttgart, Germany, Research Rep. 2017.

[3] J. Ehlbeck and F. Colling, "Biegefestigkeit von Brettschichtholz in Abhängigkeit von Rohdichte, Elsatizitätsmodul, Ästigkeit und Keilzinkung der Lamellen, der Lage der Keilzinkung sowie von der Trägerhöhe," Versuchsanstalt für Stahl, Holz und Steine, Universität Fridericiana Karlsruhe, Karlsruhe, Germany, Tech. Rep. 1987.

[4] H. J. Blaß, M. Frese, P. Glos, P. Linsenmann, and J. Denzler, "Biegefestigkeit von Brettschichtholz aus Buche," Universitätsverlag Karlsruhe, Karlsruhe, Research Rep. Karlsruher Berichte zum Ingenieurholzbau ; 1, 2005.

[5] M. Frese and H. J. Blaß, "Characteristic bending strength of beech glulam," *Materials and structures*, vol. 40, no. 1, pp. 3–13, 2007.

[6] G. Fink, "Influence of varying material properties on the load-bearing capacity of glued laminated timber," PhD thesis, ETH Zürich, 2014. DOI: 10.3929/ethz-a-010294974.

[7] A. B. Owen, "Monte carlo theory, methods and examples," in. 2013, ch. 5, pp. 7–9. [Online]. Available: http://statweb.stanford.edu/~owen/mc/.

[8] D. Kline, F. Woeste, and B. Bendtsen, "Stochastic model for modulus of elasticity of lumber," *Wood and Fiber Science*, vol. 18(2), pp. 228–238, 1986.

[9] S. Taylor and D. Bender, "Stochastic model for localized tensile strength and modulus of elasticity in lumber," *Wood and Fiber Science*, vol. 23(4), pp. 501–519, 1991.

[10] EN 408, *Timber structures – structural timber and glued laminated timber – determination of some physical and mechanical properties*, Brussels, Belgium: European Committee for Standardization, 2012.

[11] Abaqus v2017, Dassault Systèmes Simulia Corp, Johnston, RI, USA, 2017.

[12] EN 338, *Structural timber – strength classes*, Brussels, Belgium: European Committee for Standardization, 2009.

[13] E. Serrano, "Finger-joints for laminated beams. Experimental and numerical studies of mechanical behavior," Lund University, Division of Structural Mechanics, Sweden, Report TVSM-3021, 1997.

[14] G. Stapf, "Energiedissipationsfähigkeit und Ermüdungsverhalten von geklebten Holzverbindungen," Diplomarbeit, Universität Kassel, Germany, 2010.

[15] L. Blank, G. Fink, R. Jockwer, and A. Frangi, "Quasi-brittle fracture and size effect of glued laminated timber beams," *European Journal of Wood and Wood Products*, pp. 1–15, 2017, ISSN: 1436-736X. DOI: 10.1007/s00107-017-1156-0.

[16] H. J. Blaß, M. Frese, P. Glos, J. K. Denzler, P. Linsenmann, and A. Ranta-Maunus, "Zuverlässigkeit von fichten-brettschichtholz mit modifiziertem aufbau, bd. 11," Karlsruher Berichte zum Ingenieurholzbau, Karlsruhe, Germany, Tech. Rep. 2009. DOI: 10.5445/KSP/1000008462.